

Electronic Supplementary Information
for
Structural, magnetic, redox and theoretical
characterization of seven-coordinate first-row
transition metal complexes with macrocyclic ligand
containing two benzimidazolyl *N*-pendant arms

Bohuslav Drahoš,^{a} Ivana Císařová,^b Oleksii Laguta,^c Vinicius T. Santana,^c Petr Neugebauer^c and
Radovan Herchel^a*

^a *Department of Inorganic Chemistry, Faculty of Science, Palacký University, 17. listopadu 12, 771 46 Olomouc, Czech Republic, Fax: +420 585 634 954. Tel: +420 585 634 429. E-mail: bohuslav.drahos@upol.cz*

^b *Department of Inorganic Chemistry, Faculty of Science, Charles University, Hlavova 2030, 128 00 Prague, Czech Republic*

^c *Central European Institute of Technology, CEITEC BUT, Purkyňova 656/123, 61200 Brno, Czech Republic.*

Table of contents:

Figure S1. ESI mass spectra of **L** and studied complexes **1–4**.

Figure S2. IR spectra of studied complexes **1–4**.

Figure S3. ¹H–¹³C *gs*-HMQC NMR spectrum of **L**.

Figure S4. ¹H–¹³C *gs*-HMBC NMR spectrum of **L**.

Figure S5. HFEPFR measurements of a powder sample of compound **2** at 4 K and 180 GHz, 321 GHz and 415 GHz.

Figure S6. In-phase χ_{real} and out-of-phase χ_{imag} molar susceptibilities for **3** at zero and non-zero static magnetic field.

Figure S7. Cyclic voltammogram of **CH₃NO₂** in **CH₃CN**.

Figure S8. Cyclic voltammogram of **L**.

Figure S9. Comparison of cyclic voltammograms of **1** and $[\text{Mn}(\text{L2})](\text{ClO}_4)_2$.

Figure S10. Comparison of cyclic voltammograms of **2** and $[\text{Fe}(\text{L2})](\text{ClO}_4)_2$.

Figure S11. Comparison of cyclic voltammograms of **3** and $[\text{Co}(\text{L2})](\text{ClO}_4)_2$.

Table S1. Crystal data and structure refinements for studied complexes **1–4**.

Table S2. Results of continuous shape measures calculations using program Shape 2.1 for compounds **1–4**.

Table S3. Parameters of one-component Debye model for **3**.

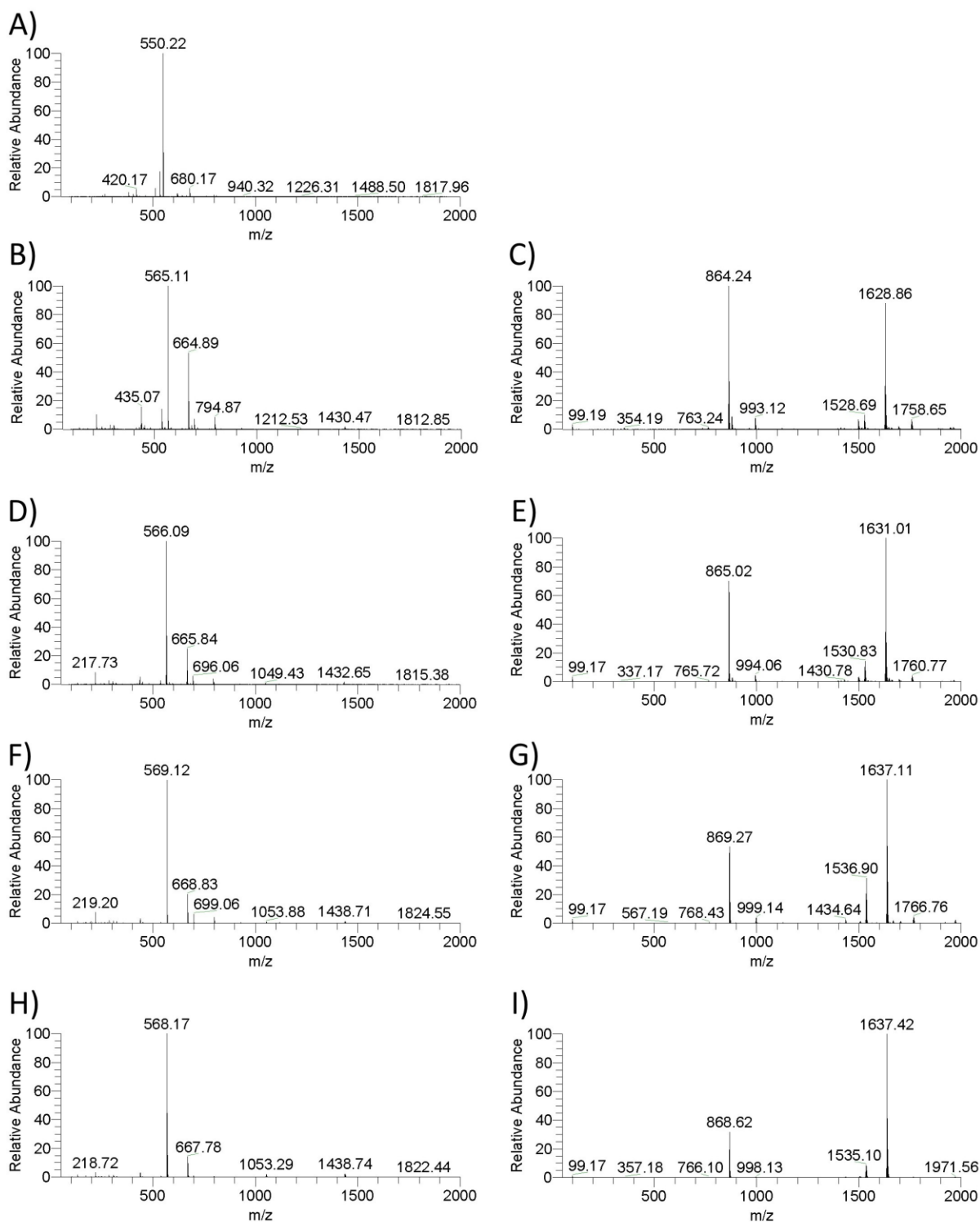


Figure S1 ESI mass spectra of the ligand **L** (A) and studied complexes **1** (B,C), **2** (D,E), **3** (F,G), **4** (H,I) (positive mode: A,B,D,F,H; negative mode: C,E,G,I).

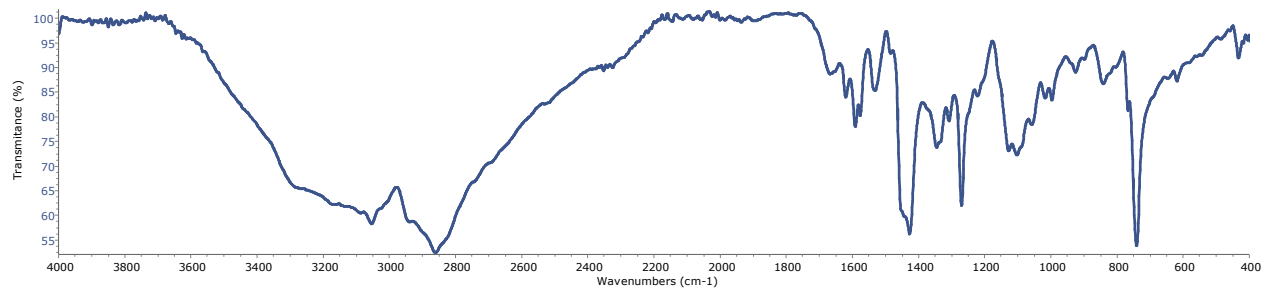


Figure S2 IR spectra of the studied ligand **L** (*dark blue*) and complexes **1** (*light blue*), **2** (*purple*), **3** (*green*) and **4** (*red*).

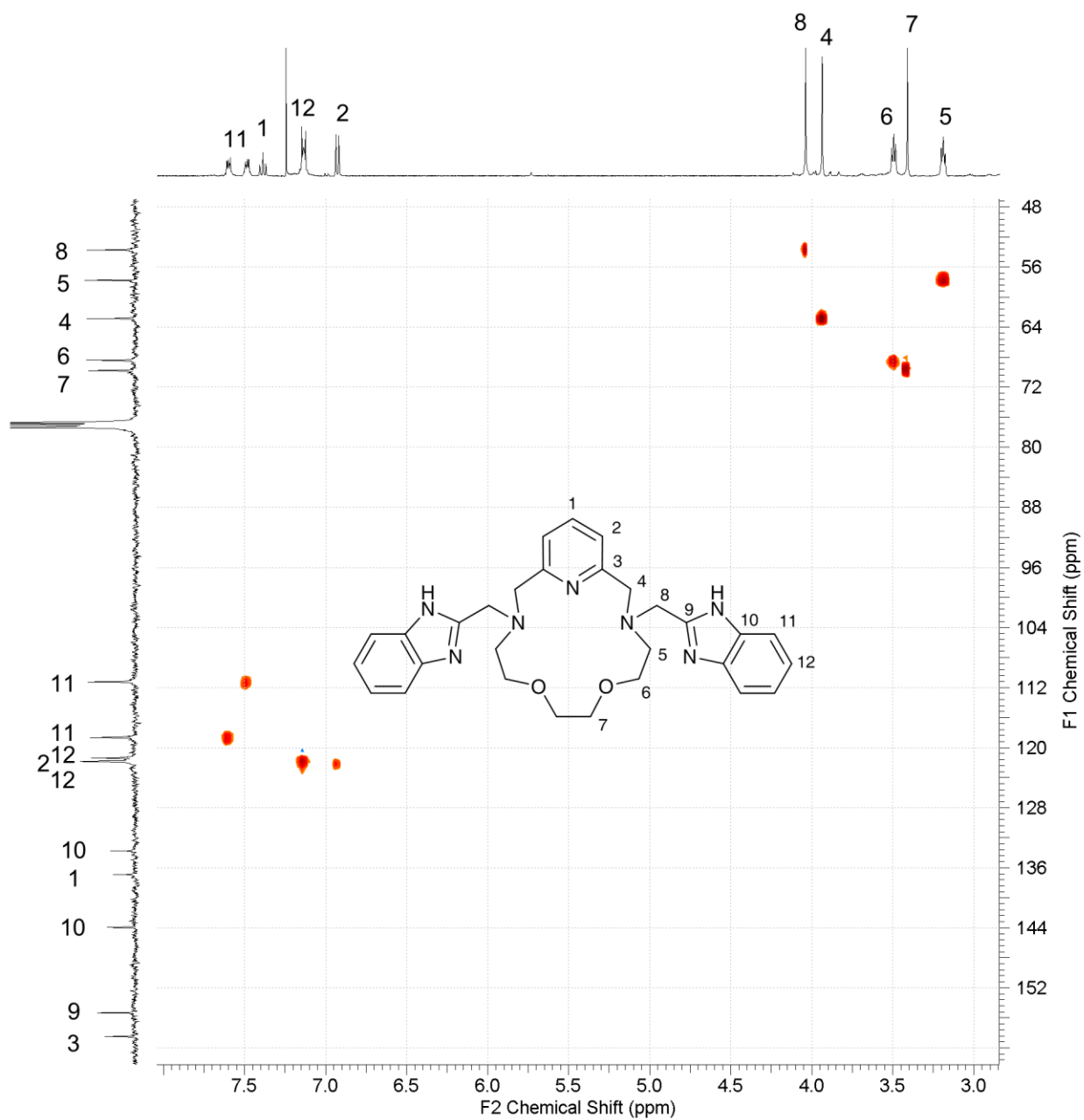


Figure S3 ^1H - ^{13}C *gs*-HMQC NMR spectrum (400 MHz, CDCl_3) of **L** (3,12-bis((1*H*-benzimidazol-2-yl)methyl)-6,9-dioxa-3,12,18-triazabicyclo[12.3.1]octadeca-1(18),14,16-triene) with the residual peak of CHCl_3 at 7.27 ppm (^1H) and CDCl_3 at 77.0 ppm (^{13}C).

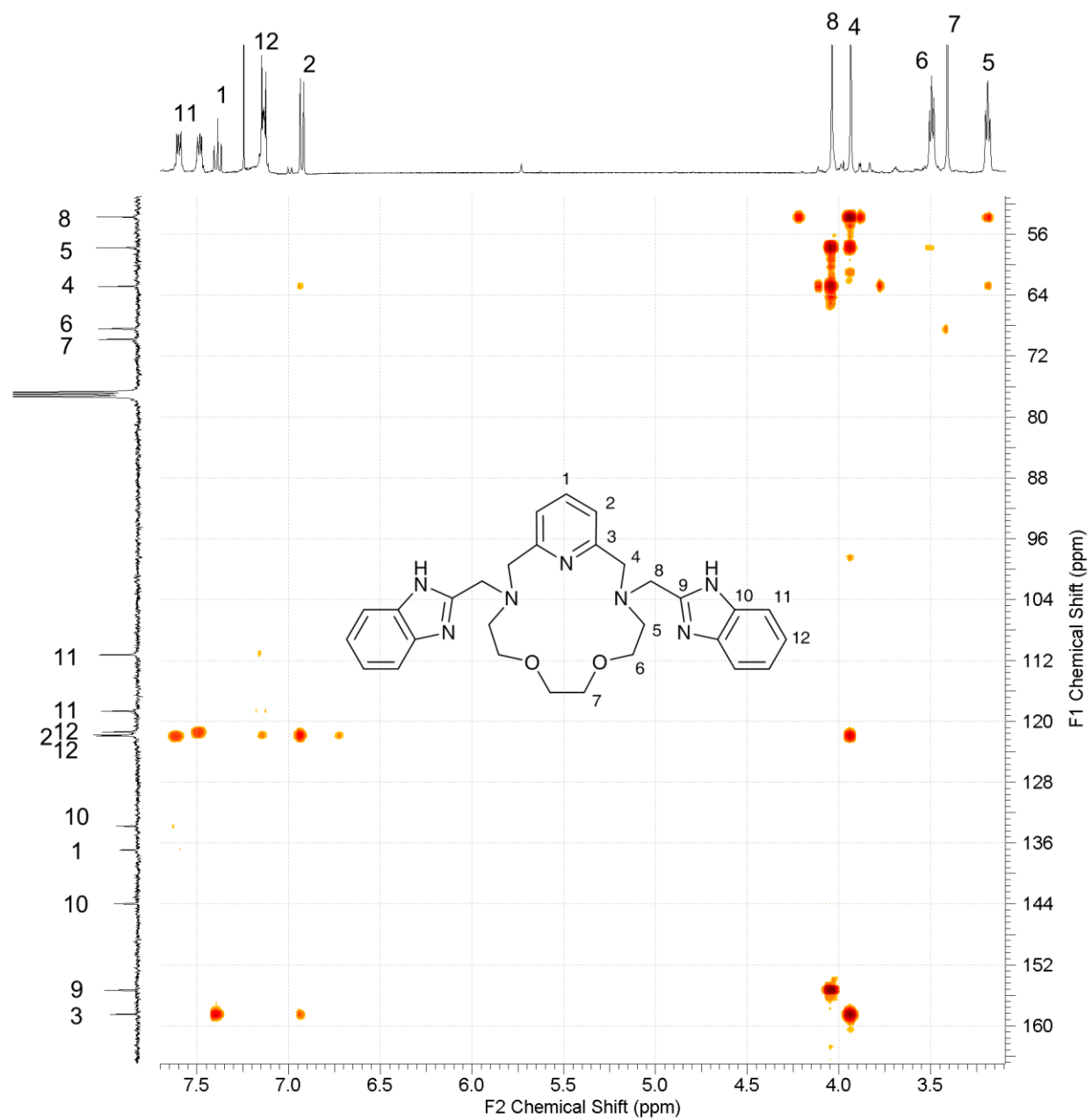


Figure S4 ^1H - ^{13}C g_S -HMBC NMR spectrum (400 MHz, CDCl_3) of **L** (3,12-bis((1*H*-benzimidazol-2-yl)methyl)-6,9-dioxo-3,12,18-triazabicyclo[12.3.1]octadeca-1(18),14,16-triene) with the residual peak of CHCl_3 at 7.27 ppm (^1H) and CDCl_3 at 77.0 ppm (^{13}C).

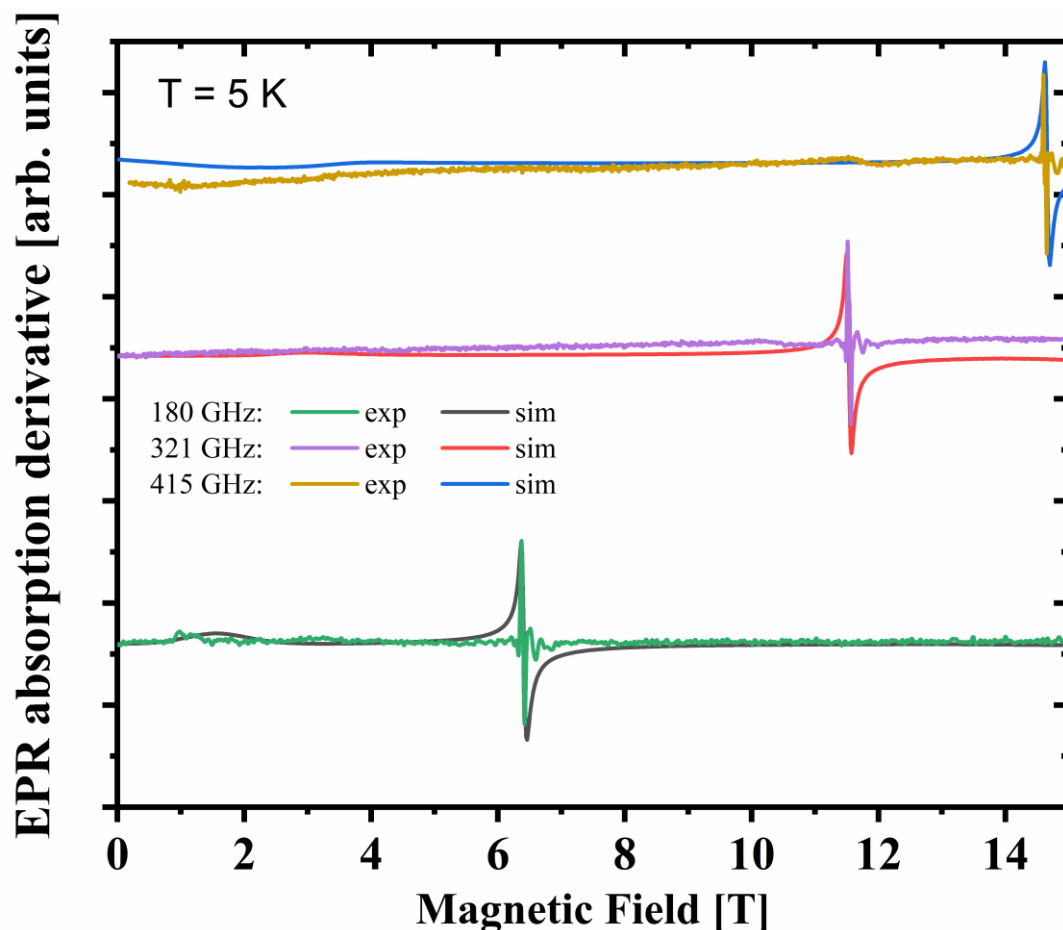


Figure S5 HFEPR measurements of a powder sample of compound **2** at 4 K and 180 GHz, 321 GHz and 415 GHz. At $T > 10$ K, there was no absorption in any of the tested frequencies (not shown), in agreement with simulated results, which present a significant decrease of the absorption intensity for a small increase in temperature. Relaxation and population of excited states determines the spectra properties at different temperatures. The simulation was performed for a spin $S = 2$ system using the CASSCF/NEVTP2 calculated g values from Table 3, but with $D = + 8.2 \text{ cm}^{-1}$ and $E/D = 0.29$. Anisotropic broadening of 50 GHz was included in the simulation in order to fit the experimental data (HStrain in the y direction coincident with the higher g value.)

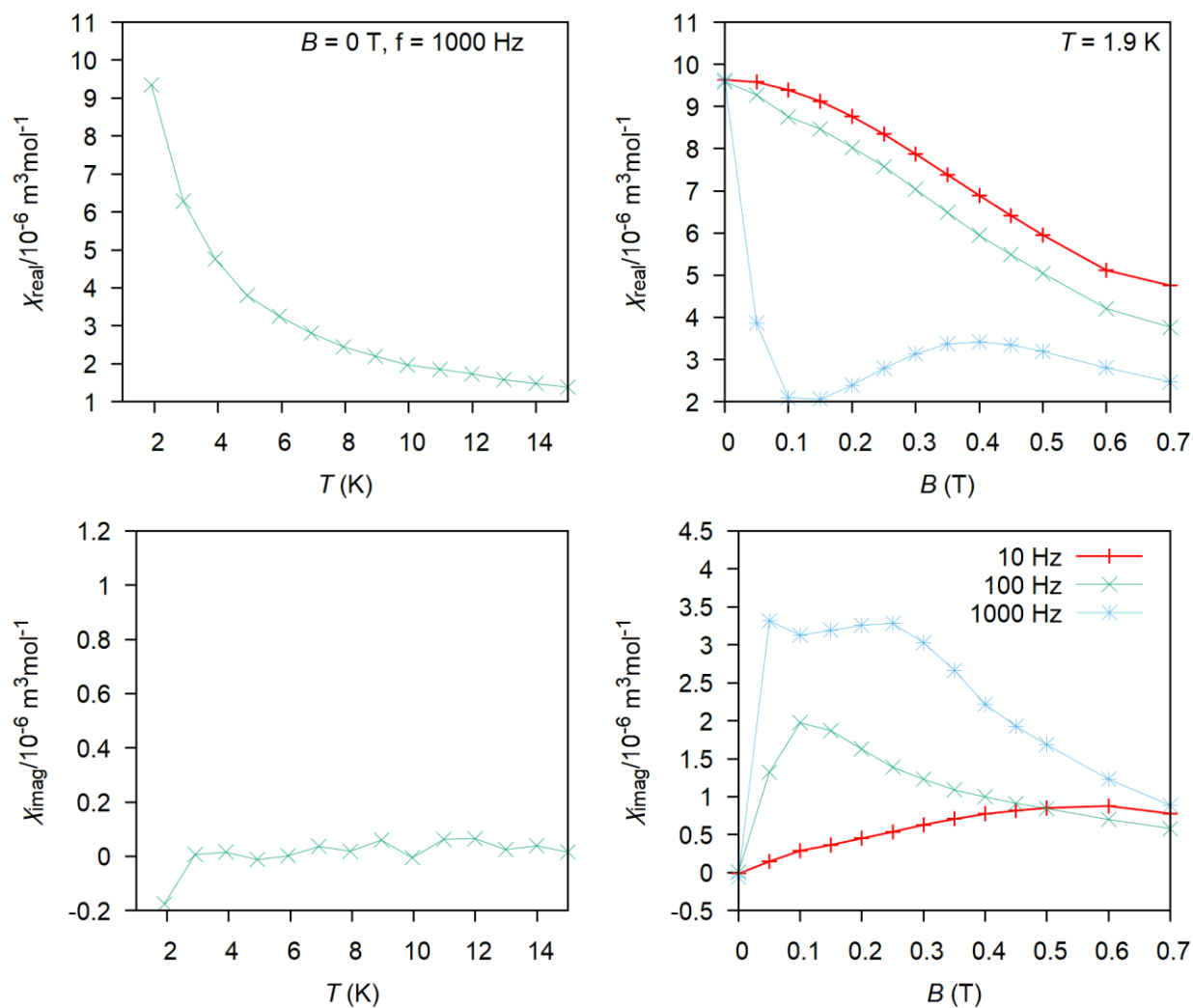


Figure S6 In-phase χ_{real} and out-of-phase χ_{imag} molar susceptibilities for **3** at zero static magnetic field (*left*) and in non-zero static field (*right*). Lines serve as guides for the eyes.

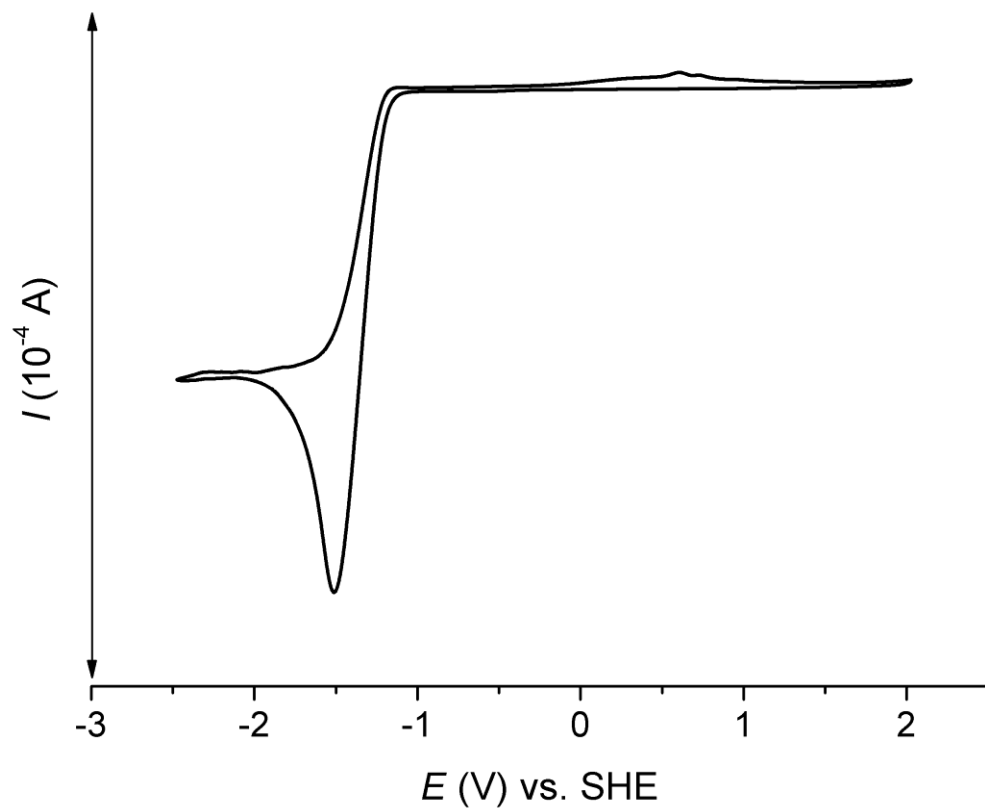


Figure S7 Cyclic voltammogram of CH_3NO_2 recorded with a glassy carbon electrode at the rate 100 mV/s using 0.1M tetrabutylammonium perchlorate as supporting electrolyte in CH_3CN under argon atmosphere.

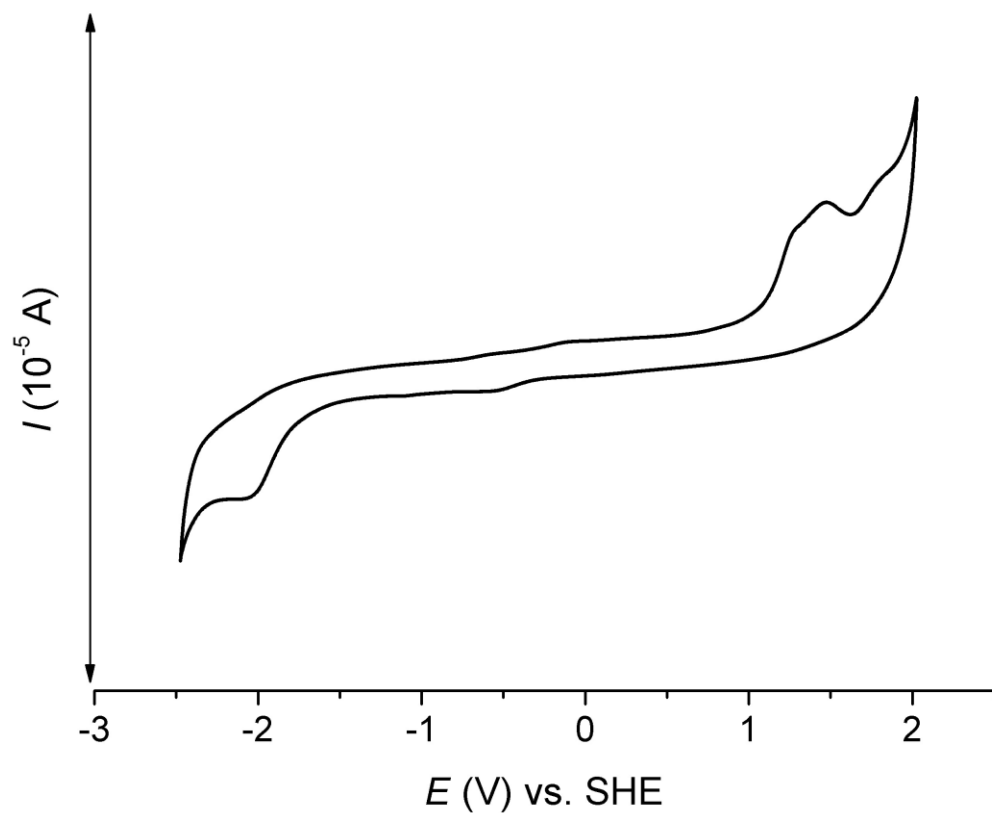


Figure S8 Cyclic voltammogram of **L** recorded with a glassy carbon electrode at the rate 100 mV/s using 0.1M tetrabutylammonium perchlorate as supporting electrolyte in CH_3CN under argon atmosphere.

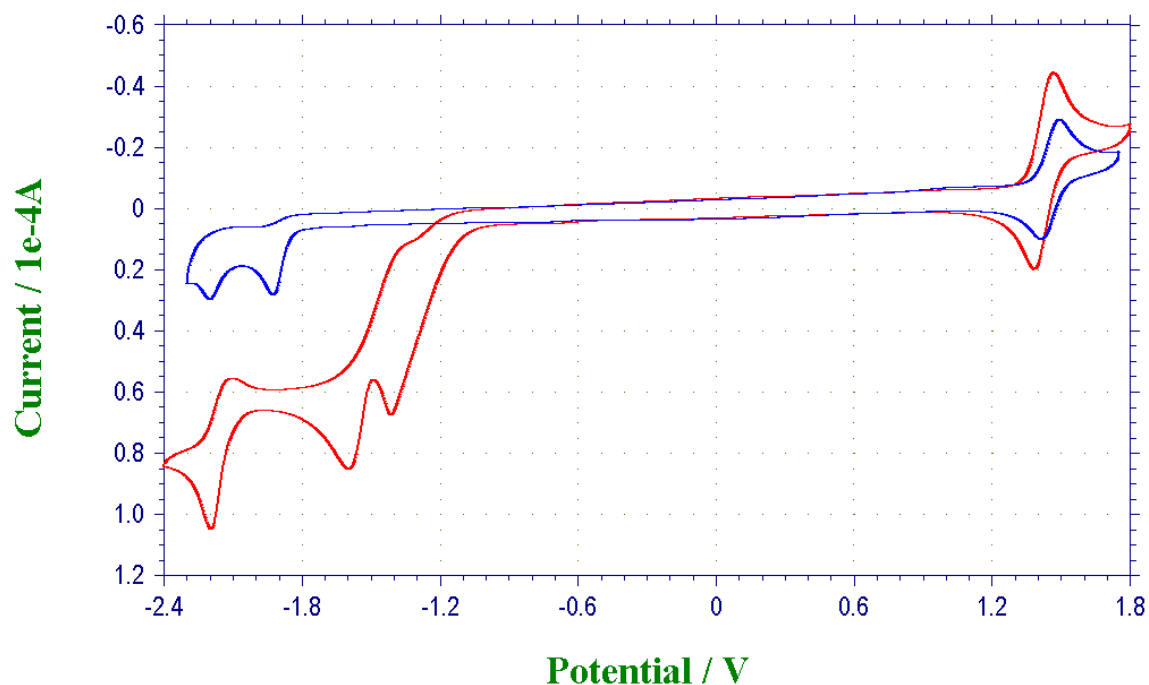


Figure S9 Comparison of cyclic voltammograms of **1** (*red*) and $[\text{Mn}(\text{L}2)](\text{ClO}_4)_2$ (*blue*) recorded with a glassy carbon electrode at the rate 100 mV/s using 0.1M tetrabutylammonium perchlorate as supporting electrolyte in CH_3CN under argon atmosphere.

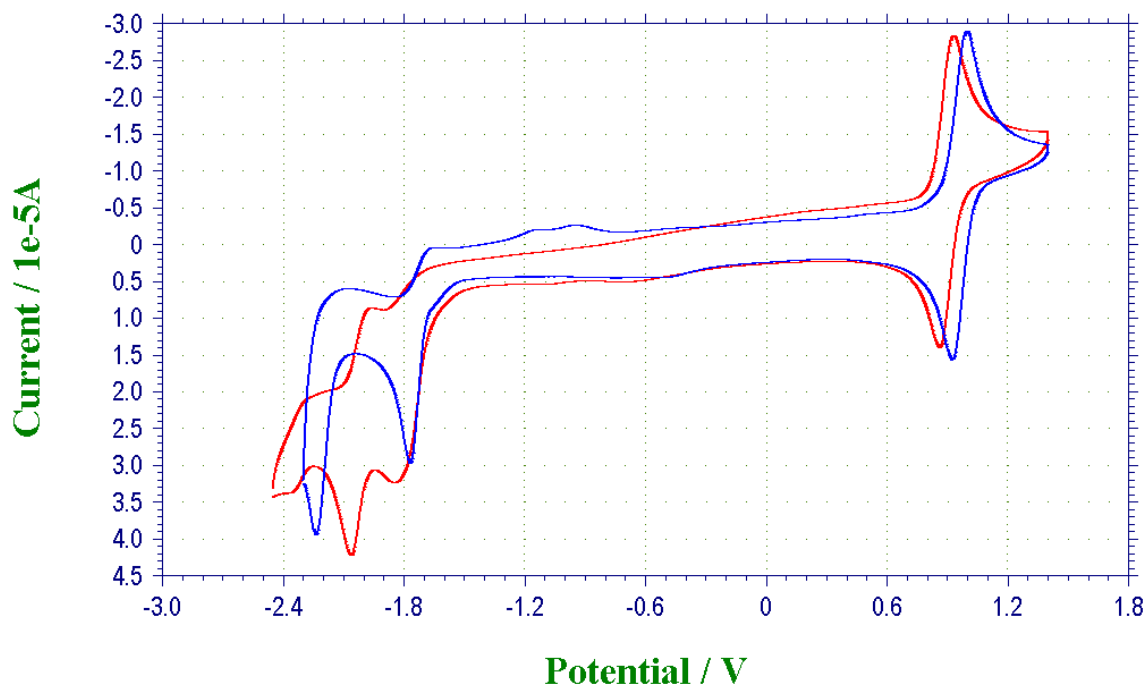


Figure S10 Comparison of cyclic voltammograms of **2** (*red*) and $[\text{Fe}(\text{L}2)](\text{ClO}_4)_2$ (*blue*) recorded with a glassy carbon electrode at the rate 100 mV/s using 0.1M tetrabutylammonium perchlorate as supporting electrolyte in CH_3CN under argon atmosphere.

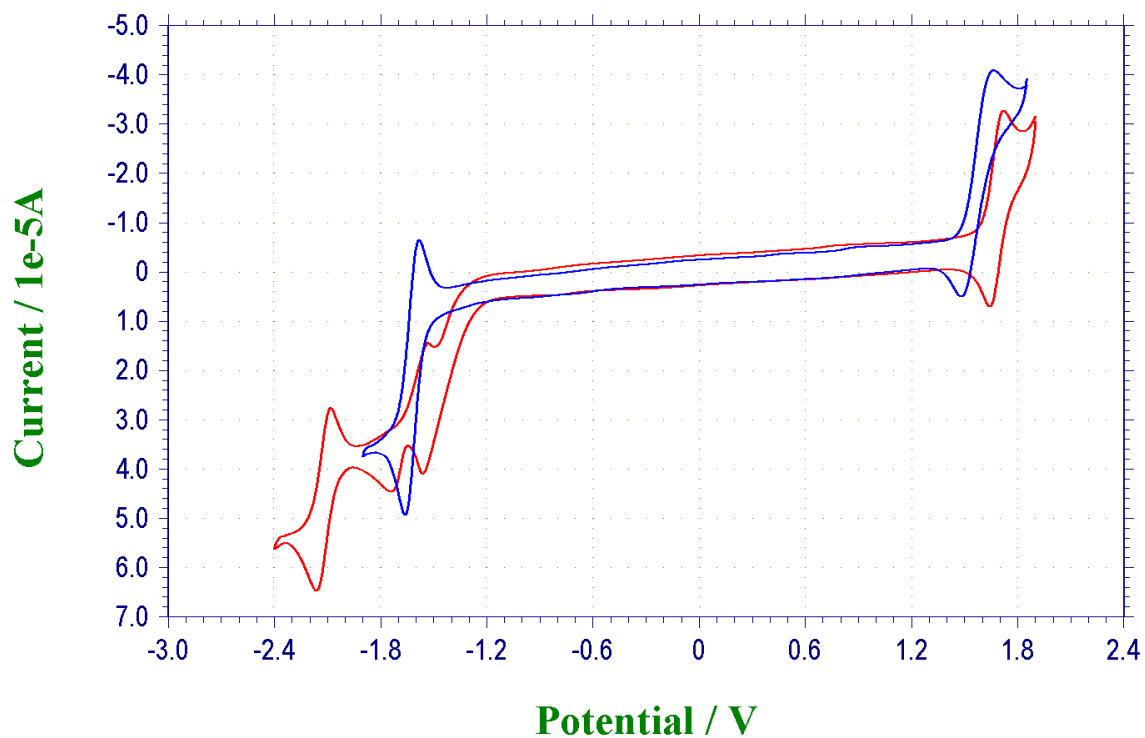


Figure S11 Comparison of cyclic voltammograms of **3** (*red*) and $[\text{Co}(\mathbf{L2})](\text{ClO}_4)_2$ (*blue*) recorded with a glassy carbon electrode at the rate 100 mV/s using 0.1M tetrabutylammonium perchlorate as supporting electrolyte in CH_3CN under argon atmosphere.

Table S1 Crystal data and structure refinements for studied complexes **1–4**.

Compound	1	2	3	4
Formula	C ₆₁ H ₇₅ Cl ₄ Mn ₂ N ₁₇ O ₂₆	C ₆₁ H ₇₅ Cl ₄ Fe ₂ N ₁₇ O ₂₆	C ₆₁ H ₇₅ Cl ₄ Co ₂ N ₁₇ O ₂₆	C ₆₁ H ₇₅ Cl ₄ Ni ₂ N ₁₇ O ₂₆
<i>M</i> _r	1714.06	1715.88	1722.04	1721.60
Temperature (K)	150(2)	150(2)	150(2)	150(2)
Wavelength (Å)	0.71073	0.71073	0.71073	0.71073
Crystal system	triclinic	triclinic	triclinic	triclinic
Space group	P-1	P-1	P-1	P-1
<i>a</i> (Å)	13.8753(4)	13.8335(4)	13.8322(4)	13.8336(4)
<i>b</i> (Å)	14.9584(4)	14.9487(4)	14.9418(4)	14.9837(4)
<i>c</i> (Å)	18.8648(6)	18.7892(5)	18.7191(5)	18.6193(5)
<i>α</i> (°)	77.3590(10)	77.1470(10)	77.1450(10)	76.9370(10)
<i>β</i> (°)	76.2910(10)	76.1020(10)	76.4180(10)	76.3470(10)
<i>γ</i> (°)	86.4830(10)	86.4130(10)	86.2140(10)	86.0280(10)
<i>V</i> , Å ³	3711.50(19)	3677.05(18)	3665.99(18)	3652.76(18)
<i>Z</i>	2	2	2	2
<i>D</i> _{calc} , g cm ⁻³	1.534	1.550	1.560	1.565
<i>μ</i> , mm ⁻¹	0.575	0.632	0.691	0.754
<i>F</i> (000)	1772	1776	1780	1784
<i>θ</i> range for data collection (°)	1.669–25.000	1.143–25.000	1.607–25.000	1.153–27.570
Refl. collected	43364	49826	38740	61058
Independent refl.	13083	12969	12915	16876
<i>R</i> (int) ^a	0.0299	0.0191	0.0284	0.0282
Data/restraints/parameters	13083 / 24/ 992	12969/42/992	12915/ 24/992	16876/0/ 994
Completeness to <i>θ</i> (%)	100.0	100.0	100.0	99.8
Goodness-of-fit on <i>F</i> ²	1.045	1.031	1.028	1.021
<i>R</i> ₁ , <i>wR</i> ₂ (<i>I</i> > 2σ(<i>I</i>)) ^b	0.0505, 0.1300	0.0535, 0.1487	0.0457, 0.1206	0.0491, 0.1278
<i>R</i> ₁ , <i>wR</i> ₂ (all data) ^b	0.0689, 0.1375	0.0590, 0.1521	0.0607, 0.1273	0.0641, 0.1371
Largest diff. peak and hole / Å ⁻³	1.125 and -1.008	1.120 and -1.196	1.034 and -0.892	1.473 and -1.012
CCDC number	1942109	1942110	1942111	1942112

$$^a R_{\text{int}} = \frac{\sum |F_o^2 - F_{o,\text{mean}}^2|}{\sum F_o^2}, ^b R_1 = \frac{\sum (|F_o| - |F_c|)}{\sum |F_o|}; wR_2 = [\sum w(F_o^2 - F_c^2)^2 / \sum w(F_o^2)^2]^{1/2}$$

Table S2 Results of continuous shape measures calculations using program Shape 2.1 for compounds **1–4**.^a

CN = 7 ^b	HP-7	HPY-7	PBPY-7	COC-7	CTPR-7	JPBPY-7	JETPY-7
1	27.978	22.283	1.653	6.447	4.998	4.625	17.671
2	28.056	22.370	1.482	6.675	5.225	4.202	18.219
3	28.986	22.755	1.208	6.699	5.117	3.806	18.889
4a ^c	29.553	22.661	1.201	6.818	5.114	3.296	20.061
4b ^c	29.760	23.638	1.112	6.559	5.109	3.232	20.354

^a the listed values correspond to the deviation between the ideal and real coordination polyhedra, the lowest values are in red color.

^b HP-7 = heptagon, HPY-7 = hexagonal pyramid, PBPY-7 = pentagonal bipyramid, COC-7 = capped octahedron, CTPR-7 = capped trigonal prism.

^c calculations were performed for two crystallographically independent molecules present in the asymmetric unit of **4**.

Table S3 Parameters of one-component Debye model for **3**.

T/K	$\chi_S/(10^{-6} \text{ m}^3\text{mol}^{-1})$	$\chi_T/(10^{-6} \text{ m}^3\text{mol}^{-1})$	α	$\tau/\text{(s)}$
1.9	0.5465	9.3676	0.0360	3.79E-04
2.1	0.4772	8.5063	0.0429	2.95E-04
2.3	0.4723	7.8689	0.0385	2.40E-04
2.5	0.4225	7.2721	0.0410	1.91E-04
2.7	0.3045	6.7651	0.0418	1.50E-04
2.9	0.2364	6.3360	0.0438	1.23E-04
3.1	0.3043	5.9433	0.0284	1.03E-04
3.3	0.4118	5.6110	0.0349	8.89E-05
3.5	0.4167	5.3075	0.0350	7.44E-05
3.7	0.5233	5.0392	0.0077	6.71E-05
3.9	0.3856	4.7989	0.0092	5.59E-05
4.1	0.5628	4.5769	0.0140	5.11E-05
4.3	0.4393	4.3766	0.0068	4.40E-05
4.5	0.6701	4.1932	0.0063	4.05E-05
4.7	0.9442	4.0325	0.0069	4.01E-05
4.9	0.9838	3.8823	0.0072	3.48E-05